[TITLE PAGE]

Title: In Rhesus monkeys, CSF-contacting neurons are the only neurons present in the medullo-spinal peri-ependymal zone.

Authors: Anne Kastner & Nicolas Wanaverbecq

Affiliation : Institut de Neurosciences de la Timone, Aix-Marseille Université (AMU) & CNRS, UMR7289, Timone Campus, 27 Boulevard Jean Moulin, 13005 Marseille, France

Corresponding author: Nicolas Wanaverbecq, nicolas.wanaverbecq@univ-amu.fr

[ABSTRACT] [247 words]

In spinal cord and medulla, ependymal cells are organized in a monolayer forming the central canal (cc). In rodents, this region, also known as a stem cell niche, was shown to contain cerebrospinal fluid-contacting neurons (CSF-cNs). These neurons are GABAergic and because of their chemo- and mechanosensory properties they would represent a novel sensory system intrinsic to the central nervous system. In primates, little is known about these neurons and more generally about the region around the cc. Here, using immunohistochemical approaches, we investigated the organization of the cc region and CSF-cN properties in *Macaca mulatta* Rhesus monkey. In contrast to rodent, we observe along the whole medullo-spinal axis a large zone around the cc delimited by long radial ependymal fibers that is enriched with astrocytes and microglia but largely devoid of neuronal elements except for CSF-cNs. These primate CSF-cNs share with rodent CSF-cNs similar morphological and phenotypical features with a largely immature profile. Our data suggest that they extend their axons in the longitudinal axis to form fiber bundles close to the cc and we further show that CSF-cNs receive GABAergic and serotoninergic synaptic contacts on their soma and dendrite. Taken together our results reveal in Rh. monkey a specific organization of the region around the cc potentially forming a buffer zone between CSF from parenchyma where CSF-cNs would play a crucial role in the detection of CSF signals and their transmission to the central nervous system, a role that would need to be further investigated.

[INTRODUCTION] [780 words]

Along the medullo-spinal axis, a monolayer of ependymal cells (EC) forms the central canal (cc) wall and separates cerebro-spinal fluid (CSF) from parenchyma. Ependymal cells selectively express vimentin with markers of stem cells (nestin, Sox2, 3CB2 and FoxJ1) (Meletis et al., 2008; Hamilton et al., 2009; Marichal et al., 2012) and this region is therefore considered as a stem cell niche where reparatory and regenerative processes have been reported following lesion (Sabelström et al., 2013). Interestingly, close to and within the EC layer (ECL) neurons in contact with the CSF are also found and exhibit a characteristic morphology and phenotype that is conserved in all vertebrates (Agduhr, 1922; Bruni and Reddy, 1987; LaMotte, 1987; Stoeckel et al., 2003; Vígh et al., 2004; Marichal et al., 2009; Djenoune et al., 2014; Orts-Del'Immagine et al., 2014) . These CSF-contacting neurons (CSF-cNs) are bipolar GABAergic cells, they extend a single large dendrite toward the cc ended with a protrusion or 'bud' in contact with the CSF and their axon regroup in the ventral region of the spinal cord (SC) to form large bilateral horizontal fiber bundles (Stoeckel et al., 2003; Djenoune et al., 2017; Jurčić et al., 2021; Gerstmann et al., 2022). CSF-cNs selectively express the polycystin kidney disease 2-like 1 (PKD2L1) ion channel, a member of the transient potential receptors (TRP) superfamily with sensory properties (Djenoune et al., 2014; Jalalvand et al., 2014; Orts-Del'Immagine et al., 2014; Petracca et al., 2016). In adult animals, they further exhibit an incomplete neuronal maturity state with a persistent expression of doublecortine (DCX) and the homeobox transcription factor Nkx6.1, two markers of immature neurons and neuroblasts, paralleled by a low expression of neuronal nuclear protein (NeuN), a marker of mature neurons (Sabourin et al., 2009; Kutna et al., 2013; Orts-Del'Immagine et al., 2014, 2017). At the functional level, CSF-cNs were shown to exhibit a spontaneous unitary current activity carried by PKD2L1 (Orts Del'Immagine et al., 2015; Jalalvand et al., 2016a; Sternberg et al., 2018; Orts-Del'Immagine et al., 2020) and modulated by changes in extracellular pH and osmolarity (chemoreception) (Orts

Del'Immagine et al., 2015; Jalalvand et al., 2016a) as well as CSF flux and SC bending (mechanoreception) (Böhm et al., 2016; Jalalvand et al., 2016b; Sternberg et al., 2018; Orts-Del'Immagine et al., 2020). Therefore, CSF-cNs were suggested to represent a novel sensory system intrinsic to the central nervous system. This sensory function was confirmed in behavioral study in the zebrafish larva where CSF-cN selective activation led to a state-dependent modulation of locomotor activity (Fidelin et al., 2015; Hubbard et al., 2016) and more recently in the mouse where CSF-cNs appear to participate in the modulation of postural motor control (Gerstmann et al., 2022; Nakamura et al., 2023).

In non-human primates only little information is available about the region around the spinal cc (Becker et al., 2018). Nevertheless, in Macaca , EC in the lateral part of the cc were shown to be multiciliated while in the ventral and dorsal region they are uni- or biciliated, express nestin and are capable of proliferating (Alfaro-Cervello et al., 2014). CSF-cNs were also observed in this model (LaMotte, 1987; Alfaro-Cervello et al., 2014; Djenoune et al., 2014) and were shown to express PKD2L1 and markers of GABAergic neurons (Djenoune et al., 2014) or the vasoactive intestinal peptide (VIP) (LaMotte, 1987). Nevertheless, the whole organization of these neurons and of the cc zone remains largely unknown. Therefore, to better understand the whole organization of the cc region as well as CSF-cN properties and phenotype along the antero-posterior axis in primates dedicated studies are necessary.

Here, we show that in *Macaca mulatas* or Rhesus monkey (Rh. Monkey in the rest of the text), in contrast with rodents, the parenchyma is separated from the cc by a large hyponeuronal zone containing long radiating EC fibers and enriched with astrocytes and microglia forming a peri-ependymal zone (PEZ). This PEZ is observed along the whole medullo-spinal axis with conserved properties and the only neurons present in this area are CSF-cNs. Further, CSF-cNs exhibit similar morphological properties as in rodents and show expression of immaturity markers but lack the classical maturity ones. Their axon appear to form horizontal fiber bundles

around the cc while GABAergic and serotoninergic, but not glutamatergic or cholinergic, synaptic contacts are observed on CSF-cN soma and dendrite. Taken together our results indicate the presence in Rh. monkey of a zone around the cc where astrocytes and ependymal cell fibers would act as a buffering zone for circulating bioactive signals between CSF and parenchyma, while CSF-cNs would play a crucial role in the detection of these signals and their transmission to the central nervous system, a role that would need to be further investigated.

[RESULTS] [5159 words]

1. The region around the central canal forms a hyponeuronal astroglial zone.

We first analyzed the organization of the region around the Rh. monkey central canal (cc) at the cervical (C7/C8) SC level and look for the distribution of EC and fibers, neuronal cell bodies, dendrites, and axons as well as astrocytes. Labelling against vimentin (Vim) indicates as expected the presence of EC only around the cc (Fig. 1A_1-D_1) with their cell body forming the cc wall or ependymal cell layer (ECL) (Fig. 1A_2-D_2). In agreement with previous work (Alfaro-Cervello et al., 2014), we observed that vimentin positive fibers originating from the ECL extend radially within the white matter (WM) over long distance (~100-150 µm on both side) (Apkarian and Hodge, 1989) to form a large zone around the cc (Fig. 1A_2-D_2), called peri-ependymal zone (PEZ) in the rest of the text. Immunolabelling against the neurofilament H (NFH, non-phosphorylated form; Fig. 1A_3) or neurofilament 160 kDa (NF-160, Fig. 1B_3) reveals a strong immunoreactivity (IR) in the whole grey matter (GM) and a more diffused one in the white matter (WM) (Fig. 1A_3 and B_3). Surprisingly, only rare neuronal elements are visible in the PEZ (Fig. 1A_3-A_4 for NFH and B_3-B_4 for NF-160). The merge images on the right confirm this atypical organization and indicate a neuron-free or hyponeuronal PEZ around the cc (Fig. 1A_4-B_4). Note in B3, the presence in the dorsal region of the SC of numerous NF-160 positive puncta

corresponding to longitudinal axonal projection to or from supra-spinal structures. The absence of mature neuron in the PEZ is further illustrated by immunolabelling against the neuronal nuclear protein (NeuN) indicating that neuronal cell bodies are only present outside the PEZ (Fig. 1C_3-C_4). Finally, we looked for the astrocyte distribution around and within the PEZ and our data indicate (Fig. 1D) a strong immunolabelling against the glial fibrillary acidic protein (GFAP) within the vimentine immunoreactive PEZ (Fig. 1D_3 and 1D_4). Taken together our results show that in Rh. monkey the region around the cc is in a hyponeural zone enriched with astrocytes and delimited by fibers radiating from EC cell bodies.

2. CSF-contacting neurons are the only neurons present with the Peri-ependymal zone.

In previous studies in mice, we reported that CSF-cNs do not present a high expression level for NeuN and that classical neuronal maturity markers are absent, while microtubule associated protein type 2 (MAP2) immunolabelling prove to be a very efficient marker to visualize these neurons in medullo-spinal tissues (Orts-Del'Immagine et al., 2014, 2017; Jurčić et al., 2021). We therefore performed a set of experiments using antibodies against MAP2 to look for CSF-cNs distribution and morphology around the Rh. monkey cc. In transverse SC sections at the low cervical level (C7/C8), we observed a dense MAP2 immunolabelling present in the whole grey matter that surround a region highly immunoreactive against vimentin corresponding to the PEZ (Fig. 2A_1). However, in contrast to immunolabelling against NFH or NF-160, MAP2 IR is also observed within the PEZ that selectively and exclusively labels CSF-cNs (Fig. 2A_2). These MAP2 positive CSF-cNs present the characteristic morphology with a small round soma (arrows) from which a large dendrite (arrowheads) projects to the cc ending with a protrusion in the lumen (asterisks). Although, in Rh. monkey CSF-cN morphology is similar to that observed

in rodents (LaMotte, 1987; Djenoune et al., 2014; Orts-Del'Immagine et al., 2014; Jurčić et al., 2021), they are present within the ECL, beneath it or can be localized further away from the cc with dendrite extending over longer distances (> 50 µm) (Fig. 2A_2, see also Fig. 4 and 5). Finally, CSF-cN cell bodies are surrounded by vimentin positive radial fibers and their dendrites project to the cc along these fibers (Fig. 2A_3). We further performed double immunolabelling analyses against NFH and MAP2 or β3-tubuline (Tuj1; β3-Tub), a marker against cytoskeletal microtubules in the somato-dendritic and axonal compartments and confirm that the PEZ represents an hyponeural region where only CSF-cNs are present (Fig. 2B_1) and indicate that β3-tubuline also allows to selectively visualized CSF-cNs within the PEZ (Fig. 2B_2). Next, we looked for the microglia distribution within the SC tissue and reveal a strong IR against the ionized calcium-binding adaptor molecule 1 (Iba1), a selective marker for microglia (Sasaki et al., 2001), in the parenchyma (Fig. 2C). Interestingly, we also observe dense Iba1 IR within the PEZ and around the cc where Iba1 positive fibers can be visualize crossing the ECL towards the lumen (full arrows in Fig. 2C) or close to MAP2 positive CSF-cN fibers. The PEZ is therefore a region delimited by vimentin positive radial fibers enriched with astrocyte and microglia where the only neurons present are CSF-cNs. Longitudinal sections further confirm this unique PEZ organization delimited on its edge by the parenchyma (strong IR against MAP2; Fig. 2C_1), while MAP2 positive CSF-cNs are distributed at high density within the PEZ along the cc with their dendrite projecting perpendicular to the longitudinal axis (Fig. 2D_1) parallelly to vimentin positive fibers originating from EC cell bodies (Fig. 2D_2). Next, in agreement with earlier reports in fish and mouse (Djenoune et al., 2014; Orts-Del'Immagine et al., 2014; Jurčić et al., 2021), CSF-cNs selectively express PKD2L1 (although PKD2L1 IR is low) (Fig. 2E) and are GABAergic (GAD67, Fig. 2F). To confirm whether the organization observed in Rh. monkey for the region around the cc is specific to this animal model, we repeated a set of experiments in SC sections obtained from mice and rats. In contrast to the data obtained in Rh. monkey, we did not observe a

specific PEZ in rodent tissues rather the cc appears directly in contact with both astrocytes (GFAP, Fig. $3A_1$ and $3B_1$) and neuronal elements (NFH, Fig. $3A_2$ and $3B_2$). Further, in rodent vimentin positive radial fibers extend from the ECL within MAP2 positive elements in the parenchyma (Vim, Fig. $3C_1$ and $3D_1$ and MAP2, Fig. $3E_1$ and $3F_1$) and surround PKD2L1 positive CSF-cNs (PKD2L1, Fig. $3C_2$ and $3D_2$). Finally, and in contrast to the situation observed in Rh. monkey, immunolabelling against NeuN in rodent tissues reveals the presence of neurons contiguous to the cc (Fig. $3E_2$ and $3F_2$). Altogether, these results indicate that, in Rh. monkey, CSF-cNs exhibit similar morphological and phenotypical features than in rodent. However, in this primate model, the region around the cc in characterize by a unique PEZ where CSF-cNs are the only neurons present.

3. PEZ and CSF-cN organization and properties along the rostro-caudal axis of the central canal.

According to previous reports, the whole ~~spinal cord~~ SC size and grey matter shape vary along the different rostro-caudal spinal cord levels (Apkarian and Hodge, 1989) and this organization observed at the cervical level is conserved along the whole cc axis, we performed histological and quantitative analysis of the regions around the cc from the medulla to the sacral segments (Fig. $4A_1$ to $4E_1$). Our results indicate that the PEZ anatomy is conserved at all medullo-spinal segments and that neuronal elements identified with immunolabelling against NFH surround a large zone around the cc that is selectively enriched with astrocytes (GFAP, Fig. $4A_2$ to E_2). When considering the PEZ and cc orientation and shape in the segments of interest, we noted that both extended in the dorso-ventral axis at the medulla, mid-cervical as well as in the lumbar and sacral segments (Fig. 4). In contrast, at the high-cervical (Fig. 4B), low-cervical (Fig. 1) and thoracic (Fig. 4C) levels, the PEZ and cc were rather oriented in the

horizontal axis. We next looked for the presence of CSF-cNs in the PEZ in the same segments using staining against MAP2, and our data confirm first that CSF-cNs are present in the PEZ along the whole rostro-caudal axis of the cc but more importantly that they are the only neuronal population in these regions (Fig. $4A_3$-E_3). When looking more closely at CSF-cN distribution in the different segments, our results suggest a differential organization. At the medullar and cervical levels, CSF-cNs are mainly found within the PEZ (Fig. $4A_3$ and $4A_4$) at various distance from the ECL, while from thoracic to sacral segments, CSF-cNs are mostly found near or within the ECL or in a dorso-ventral position (Fig. $4C_3$ to $4E_3$ and $4C_4$ to $4E_4$).

To further characterize the organization of the PEZ in our study, we performed a quantitative analysis for the PEZ and cc anatomy as well as of CSF-cN distribution (Fig. 5 and Table 1). First, we measured from the medullar to the sacral levels the PEZ width and we indicate that it is the largest around 80 µm at the medullar and caudal cervical levels (Med and cCerv; Fig. 5A and Table 1A). The PEZ width is smaller at the rostral and mid-cervical (around 50 µm; rCerv and mCerv) and further decreases at more caudal segments to be around 30 µm (from thoracic to sacral segments). Next, we analyzed the cc area (Fig. 5B) at the same levels of interest and found the higher values at the medulla (Med) and sacral (Sac) levels (around 7 x 10^3 μm^2). In more caudal regions between the rostral cervical and lumbar segments, the cc area ranges from 3 to 5 x 10^3 μm^2 with no significant differences (Fig. 5B and Table 1B; see Fig. legend for details). We further analyzed the CSF-cN density (Fig. 5C and Table 1C; number of CSF-cNs/10 µm tissue depth) along the rostro-caudal axis of the cc and found the largest cell density at the mid and caudal cervical levels (Fig. 5C; cell number between 10 and 15) compared to the other segments where the density is on average around 8 CSF-cNs (Fig. 5C and Table 1C; see Fig. legend for details). Finally, regarding their distance to the cc (*i.e.* the length of their dendrite), our measurements indicate that CSF-cN cell bodies are on average at 50 µm from the cc in the medulla and cervical regions, *i.e.* the most rostral zones, except at the

mid-cervical level where CSF-cNs are significantly closer (Fig. 5D and Table 1). In more caudal segments, CSF-cNs are found closer to the cc although with a larger variability and an average distance around 20 to 25 µm (Fig. 5D and Table 1). In the more anterior segments (Med and Cerv), CSF-cNs could be found at distance as high as 100 µm right at the edge of the PEZ (see Fig. $2A_2$ and $2B_1$), however at all levels, CSF-cNs are distributed in the whole PEZ as well as within the ECL (intra-ependymal). Note that due to the maker used (MAP2) to visualize CSF-cNs and perform the quantification, one cannot exclude the presence of CSF-cNs within the parenchyma. Altogether, our results indicate that the PEZ and cc anatomy varies along the rostro-caudal axis with the widest PEZ and larger cc observed mostly in the anterior segments. This anatomy is accompanied by CSF-cNs at a higher density and larger distance to the cc for the same anterior segments.

4. In Rh. monkey, CSF-cNs present a similar phenotype as in rodents and exhibit an intermediate neuronal maturity.

In rodents, CSF-cNs are known to exhibit a low/intermediate neuronal maturity state (Orts-Del'Immagine et al., 2014, 2017; Petracca et al., 2016; Jurčić et al., 2021) characterized by the absence or low levels of NeuN (a marker for mature neurons) and the expression of doublecortin (DCX, a marker of immature neurons) along with Nkx6.1 expression (a homeobox transcription factor expressed in neuronal cells at early developmental stages and only conserved in some neural progenitors of the ventral spinal neuroepithelium in adult animals) (Sabourin et al., 2009; Kutna et al., 2013; Orts-Del'Immagine et al., 2014, 2017). To date, little is known about CSF-cN phenotype and maturity state in Rh. monkey. We reported above the absence of NeuN immunolabelling within the PEZ (see Fig. 1C) but to further explore CSF-cNs maturity state in Rh. monkey, we performed a set of immunohistofluorescence experiments

using classical markers. Here, we carried out double immunostaining against MAP2 (to visualize CSF-cNs) and NeuN to assess its level of expression selectively in CSF-cNs. Our results confirm the absence of NeuN IR within the PEZ (Fig. $6A_1$) and further indicate that CSF-cNs in Rh. monkey do not express NeuN (Fig. $6A_2$ and see inset). We next looked for DCX (Fig. 6B) and Nkx6.1 (Fig. 6C) expression in CSF-cNs and our data reveal that, in Rh. monkey, CSF-cN do express both immaturity markers. The selective Nkx6.1 expression in CSF-cNs is further confirmed by the co-immunolabelling against PKD2L1 and Nkx6.1 observed in this neuronal population (Fig. 6D).

The immature phenotype for CSF-cNs is further supported by the staining against Sox2, a stem cell marker, observed in the nuclei of this neuronal population only although at an apparent lower level than in EC (Fig. 6E and F). We next looked for expression of p27Kip1, a marker of cell cycle arrest known to be expressed in neuroblasts and observed high IR in Rh. monkey CSF-cN nuclei while it appears lower in EC (Fig. 6G). In contrast, the pattern determinant Pax6 was expressed in Vimentin positive EC but not in CSF-cNs (Fig. 6H). Altogether, our data indicate that in Rh. monkey CSF-cNs do not express maturity markers but rather several proteins classically present in non-mature neurons or neuroblasts.

5. CSF-cN axonal projection and synaptic contacts.

Here, we explored the projection path of putative CSF-cN axon in the SC tissue as well as looked for synaptic contacts on CSF-cNs. Since our data indicate that CSF-cN axon are not labelled with NFH or NF-160, two classical axonal markers (see Fig. 1 and 2), we performed our analysis using double immunolabelling against β3-tubuline (β3Tub) and MAP2. Indeed β3Tub is an element of cytoskeletal microtubules, present both in the somato-dendritic and axonal compartments, while MAP2 only labels soma and dendrites. This approach, therefore, allows to

distinguish the somato-dendritic from the axonal compartments and to visualize axonal projection arising from CSF-cN cell bodies within the PEZ (Fig. 7). Our data on transverse spinal cord sections reveals puncta or patches within the PEZ and adjacent to the ventral ECL that are MAP2 negative but β3Tub positive and therefore most likely correspond to axons that were cut in the section process (white arrowhead in Fig. 7A_{1-2} and Fig. 4). We next analyzed MAP2/β3tub immunolabelling on longitudinal SC sections across the cc region to confirm this observation and as expected, we could observe MAP2 positive/β3Tub positive CSF-cNs soma and dendrites within the PEZ (Fig. 7A_{3-4}) but also MAP2 negative/β3Tub positive rostrocaudal fibers that were either isolated or aggregated as fiber tracts (white arrowhead in Fig. 7A_4 and see also B-D). To confirm our results, we repeated on transverse and longitudinal sections experiments using double immunolabelling against β3Tub and NFH (Fig. 7B) or NF-160 (Fig. 7C). As previously reported, we observed high NF-160 (Fig. 7B) and NFH (Fig. 7C) IR mainly outside the PEZ however the β3Tub positive fibers/ patches were never NF-160 or NFH positive (Fig. 7B and C). Note on the transverse section illustrated in Fig. 7B_2 occasional NF-160 positive elements present in the ventral and dorsal PEZ as well as the dense NF-160 positive puncta in the dorsal region of the SC that correspond to ascending or descending axonal projection tracts. Our results, in agreement with the intermediate maturity state reported for Rh. monkey CSF-cNs (see above) and the previous studies in rodents (Orts-Del'Immagine et al., 2014, 2017), suggest that their axon do not express mature axonal markers and would project in the longitudinal axis within the PEZ. To test whether CSF-cNs receive synaptic contacts despite their low maturity state, we analyzed the presence of synaptophysin labelling on MAP2 positive CSF-cNs and explored the phenotype of the identified contacts (Fig. 8). Our results for the cervical segments indicate the presence of synaptophysin positive puncta along CSF-cN dendrites (Fig. 8A) within the PEZ and on their soma but not intra-ependymally. In the thoracic and lumbar regions, most CSF-cNs are intra-ependymal and in these segments, the synaptophysin positive synaptic

contacts are mainly observed on CSF-cN cell bodies (Fig. 8B). The orthogonal projections illustrated in Fig. 8A_2 and B_2 further support this anatomical organization and indicate that the synaptophysin positive contacts form dense IR puncta along the dendrites and surrounding the whole structure or are present on the soma. To specify the nature of the synaptic contact CSF-cNs receive, we tested the colocalisation of synaptophysin with markers of cholinergic (ChAT), GABAergic (GAD67), glutamatergic (vGlut1) and serotoninergic (5-HT) neurons. GAD67/synaptophysin double immunolabelling reveals that numerous synaptophysin positive elements contacting CSF-cNs were GABAergic (Fig. 8C_{1-2}). Similarly, MAP2/5-HT/ synaptophysin immunolabelling shows that 5-HT fibers are present in the PEZ, mainly in its dorsal part and that they are often colocalized with synaptophysin on CSF-cN soma and dendrites (Fig. 8D_{1-3}). In contrast, although we observe ChAT or vGlut1 positive fibers or soma in the parenchyma with some rare fibers arriving in the PEZ, we never visualize on CSF-cNs synaptophysin positive structure that were also IR for ChAT or vGluT1 (Data not shown). To summarize, CSF-cNs do receive synaptic contacts that are restricted on the somato-dendritic compartment in the PEZ but not within the ECL. These contacts appear to be GABAergic and serotoninergic but not glutamatergic nor cholinergic.

[DISCUSSION] [1606 words]

Our analysis of the cc region in Rh. monkey highlights the presence of a large PEZ delimited by radial fibers originating from ependymal cells and enriched with astrocytes and microglia. Further, the PEZ is so-called hyponeural with the sole presence of CSF-cNs. This peculiar organization of the region around the cc that extend throughout the entire medullo-spinal axis appears specific to Rh. monkey and represent a major distinction with that observed in rodents. Nevertheless, in Rh. monkey CSF-cNs show a conserved morphology and exhibit an immature phenotype in agreement with the reports in rodents. We finally indicate that these neurons

receive on their somato-dendritic compartment synaptic contacts from GABAergic and serotoninergic terminals but not cholinergic or glutamatergic ones.

1. CSF-cNs specific properties are conserved in Rh. monkey

In agreement with previous studies (LaMotte, 1987; Alfaro-Cervello et al., 2014; Djenoune et al., 2014), we show that CSF-cNs are present around the cc in Rh. monkey. Although they are only poorly and partially detectable with PKD2L1 antibodies, they are clearly labelled with antibodies against MAP2 and β3-Tub. A similarity between rodent and Rh. monkey CSF-cNs is also their GABAergic phenotype as indicated by GAD67 IR (Orts-Del'Immagine et al., 2014; Djenoune et al., 2017; Jurčić et al., 2021) and morphology. As in mice, CSF-cNs in Rh. monkeys have a small ovoid shape and extend a dendrite toward the cc, with a terminal bud in contact with the CSF. Moreover, we show that they are present in Rh. monkey along the whole medullospinal axis at various distances from the cc depending on the rostrocaudal level. Thus, CSF-cNs are more distant from the cc at rostral levels (medulla and cervical levels) and closer at thoracic and lumbar levels. Such difference in CSF-cNs distribution along the rostrocaudal and dorsoventral axes has also been described in rodents (Orts-Del'Immagine et al., 2014, 2017) and one could hypothesize that this may be related to a functional heterogeneity and specific projection path as reported in zebrafish (Djenoune et al., 2017). CSF-cNs in the medulla and cervical regions were generally more distant from the cc in Rh. monkey than in mice, although a population of distal PKD2L1+ neurons have been recently described in the mouse SC (Tonelli Gombalová et al., 2020; Jurčić et al., 2021) notably in the ventral region.

In Rh. monkey alike in rodents, CSF-cNs exhibit properties of classical neurons, illustrated by MAP2 expression, synaptic contacts, neurotransmitter production (GAD67+). Nevertheless, they do not express NeuN, NF-160 or NFH classically found in mature neurons but instead we

observe expression of DCX, Nkx6.1, Sox2, p27Kip1, all proteins characteristic of neuroblasts or immature neurons. Again, this as previously shown in rodents (Stoeckel et al., 2003; Sabourin et al., 2009; Kutna et al., 2013; Orts-Del'Immagine et al., 2014, 2017). This incomplete maturity profile appears a common feature for CSF-cNs in all analyzed vertebrates. Some characteristics of juvenile neurons have also been observed at the functional level in mice using electrophysiological recordings (Jurčić et al., 2019).

Although it has been shown in rodents that CSF-cNs are not generate following post-natal or adult neurogenesis (Marichal et al., 2009; Kutna et al., 2013), they may conserve some features and functions of juvenile neurons during the adult stage. Such unique characteristic for CSF-cNs has been related to their environment in the ependymal stem cell niche and potentially their contact with the CSF. Thus, in Rh. monkey CSF-cNs are surrounding the ECL where their dendrites follow the radiating ependymal fibers. Such preferential link between CSF-cNs and ependymal cells/fibers has also previously been shown in rodents, even for distal PKD2L1+ neurons that are mostly aligned along the ventral ependymal fibers (Jurčić et al., 2021). This unique feature for CSF-cNs, together with their low-mature phenotype, reinforce the hypothesis for a function as a constitutive element of the stem cell niche along with their chemosensory and mechanosensory function. It further raises the question of whether they could be activated following SC injury and recruited in regenerative processes. To date this is an unresolved issue in mammals and dedicated studies demonstrating CSF-cN activation in these situation need to be conducted.

2. A specific astroglial peri-ependymal compartment for CSF-cNs in primates

In rodents, CSF-cNs are mostly located within the ECL or just beneath (subependymal zone) in an area containing astrocytes but also other types of neurons (Djenoune et al., 2014; Orts-

Del'Immagine et al., 2014). In contrast, we show that in Rh. monkeys CSF-cNs are the only neurons to occupy a specific and wide hyponeuronal PEZ, which is almost completely devoid of other neuronal elements as revealed by the absence of/low immunolabelling against NeuN, NFH and NF-160 within this zone as well as MAP2+ staining in the parenchyma at the boundary of the PEZ. Due to this specific anatomical organization for CSF-cNs, MAP2 can be considered as a suitable marker for these neurons in primates since it allows revealing almost the whole population of CSF-cNs distant from 0 to 150 μm to the cc. In addition, this specific PEZ zone also contains a dense synaptic innervation on CSF-cN somato-dendritic compartment. This innervation appears mainly GABAergic and could represent at least partially recurrent synaptic contacts between CSF-cNs as recently demonstrated in mice (Gerstmann et al., 2022; Nakamura et al., 2023). Beside this GABAergic innervation, our data indicate that CSF-cNs, mainly in the dorsal PEZ, appear also contacted by serotoninergic fibers. Although the origin of these fibers remains to be established, this observation suggests that CSF-cNs might be under the control of supraspinal descending serotoninergic projection. It further raises the question whether CSF-cNs might be contacted by other types of peptidergic terminals. Concerning CSF-cN axonal projection, our data in Rh. Monkeys suggest that they would run within the PEZ in a rostro-caudal and horizontal orientation. This is supported by the presence within the PEZ of longitudinal fibers that were β3-Tub+ and MAP2- as well as negative to labelling against NFH/NF-160. This organization appears different from that observed in zebrafish, mice or rat, in which axon were shown to project toward the ventral fissure and form long horizontal fiber bundles (Stoeckel et al., 2003; Jurčić et al., 2021; Gerstmann et al., 2022; Nakamura et al., 2023). However, CSF-cN connectivity and the identification of their local and distal neuronal partners is far from being characterized and would need to be further addressed using specific tracing approaches.

Paralleled by the absence of neuronal elements (except CSF-cNs), the Rh. monkey PEZ is enriched with astrocytes in agreement with the study from Alfaro-Cervello and colleagues (2014). A high density of astrocytes around the ECL was also observed in mice (Jurčić et al., 2021), suggesting that these cells may play a role in the interface between the CSF and the parenchyma. Moreover, we found that the Rh. monkey PEZ also contains numerous microglial cells, with some microglial fibers surrounding and even, in some cases, crossing the ECL toward the CSF. We do not know the functional relevance for such an organization, but we can hypothesize an interaction between with astrocytes, microglia and CSF-cNs to control CSF diffusion/composition and regulate the communication between CSF and parenchyma as well as protect the neural tissue against potential toxins or pathogen agents. CSF-cNs might further serve as signal integrator to convey information about the physio-pathological state of the central nervous system. This possibility would need to be address in future dedicated studies.

3. A phylogenetic reorganization of the peri-ependymal zone?

The different cell organization of the cc environment between rodents and Rh. monkey (absence and presence of the PEZ, respectively) raises the question of the anatomical and functional evolution of this PEZ region amongst mammals, in different primate phylum and whether these data can be translated to Humans. Here we show in Rh. Monkey, a non-human primate (NHP) from the old-world and exhibiting ‘thumb-index’ grip, a specific organization of the PEZ with CSF-cNs as the only neurons present in this region. In contrast, preliminary data obtained in marmoset, a new-world NHP without grip capability, indicate a region around the cc similar to that found in rodents with CSF-cNs within the parenchyma in the ECL or sub-ependymal zone. At this stage we are not able to draw conclusion about the different organization and whether it is related to the phylum, the ability to exhibit the ‘thumb-index’ grip

(macaque *vs.* marmoset*)* or the locomotion type (bipedal versus quadrupedal). To further address this question, it is necessary to extend the characterization of the cc organization and of CSF-cN properties in other primate species. Concerning Humans and in contrast to other mammalian species, the cc is thought to be mostly occluded and disassembled, at least in adult or old subjects. It is however patent in infants and in the adult medulla and most rostral cervical region (Yasui et al., 1999; Alfaro-Cervello et al., 2014; Garcia-Ovejero et al., 2015; Becker et al., 2018). In the case of occlusion, the cc is replaced by a highly vascularized cell 'amas' constituted of bi- and multiciliated ependymal and glial cells (Alfaro-Cervello et al., 2014; Becker et al., 2018) and there is, to data, no definitive data to confirm or infirm the presence of CSF-cNs. Thus, the cell organization of the peri-cc region (putative PEZ) remains however to be characterized. Moreover, based on electron microscopic (Alfaro-Cervello et al., 2014) and transcriptomic studies (Ghazale et al., 2019), CSF-cNs have not yet been detected in Humans, although we can notice the presence of β3-Tub immunoreactive processes in the cc region (Garcia-Ovejero et al., 2015; Becker et al., 2018). Further immunohistochemical investigations using specific neuronal markers will be necessary in Human SC and medulla samples, notably with a patent cc, to putatively identify CSF-cNs and specify the PEZ organization relative to NPH and rodents.

[CONCLUSION] [134 words]

Here, we report an in-depth anatomical study for the region around cc in the Rh. monkey that appears to be also present in Human. Although highly challenging in NHP, it will be necessary in the future to pursue the characterization of the PEZ and the CSF-cN properties, identify their axonal projection and post-synaptic partners to come closer to the understanding of their function. Finally, the functional ground for this unique organization of the PEZ in Rh. Monkey

compared to rodents is unclear and would need to be further characterized. One could hypothesize that it represents a buffer zone to control diffusion of active molecules from the CSF towards the parenchyma with CSF-cNs as intrinsic sensory neurons that would serve to sense signals and convey the information to regulate the central nervous system homeostatic state.

[REFERENCES]

Agduhr E (1922) Über ein zentrales Sinnesorgan (?) bei den Vertebraten. Zeitschrift für Anatomie und Entwicklungsgeschichte 66:223–360.

Alfaro-Cervello C, Cebrian-Silla A, Soriano-Navarro M, Garcia-Tarraga P, Matías-Guiu J, Gomez-Pinedo U, Molina Aguilar P, Alvarez-Buylla A, Luquin M-R, Garcia-Verdugo JM (2014) The adult macaque spinal cord central canal zone contains proliferative cells and closely resembles the human. J Comp Neurol 522:1800–1817.

Apkarian AV, Hodge CJ (1989) Primate spinothalamic pathways: III. Thalamic terminations of the dorsolateral and ventral spinothalamic pathways. J Comp Neurol 288:493–511.

Becker CG, Becker T, Hugnot J-P (2018) The spinal ependymal zone as a source of endogenous repair cells across vertebrates. Prog Neurobiol 170:67–80.

Böhm UL, Prendergast A, Djenoune L, Nunes Figueiredo S, Gomez J, Stokes C, Kaiser S, Suster M, Kawakami K, Charpentier M, Concordet J-P, Rio J-P, Del Bene F, Wyart C (2016) CSF-contacting neurons regulate locomotion by relaying mechanical stimuli to spinal circuits. Nat Commun 7:10866.

Bruni JE, Reddy K (1987) Ependyma of the central canal of the rat spinal cord: a light and transmission electron microscopic study. J Anat 152:55–70.

Djenoune L, Desban L, Gomez J, Sternberg JR, Prendergast A, Langui D, Quan FB, Marnas H, Auer TO, Rio J-P, Del Bene F, Bardet P-L, Wyart C (2017) The dual developmental origin of spinal cerebrospinal fluid-contacting neurons gives rise to distinct functional subtypes. Sci Rep 7:719.

Djenoune L, Khabou H, Joubert F, Quan FB, Nunes Figueiredo S, Bodineau L, Del Bene F, Burcklé C, Tostivint H, Wyart C (2014) Investigation of spinal cerebrospinal fluid-contacting neurons expressing PKD2L1: evidence for a conserved system from fish to primates. Front Neuroanat 8:26.

Fidelin K, Djenoune L, Stokes C, Gomez J, Baradel A, Del Bene F, Wyart C (2015) State-Dependent Modulation of Locomotion by GABAergic Spinal Sensory Neurons. Current Biology 25:1–13.

Garcia-Ovejero D, Arevalo-Martin A, Paniagua-Torija B, Florensa-Vila J, Ferrer I, Grassner L, Molina-Holgado E (2015) The ependymal region of the adult human spinal cord differs from other species and shows ependymoma-like features. Brain 138:1583–1597.

Gerstmann K, Jurčić N, Blasco E, Kunz S, de Almeida Sassi F, Wanaverbecq N, Zampieri N (2022) The role of intraspinal sensory neurons in the control of quadrupedal locomotion. Curr Biol 32:2442-2453.e4.

Ghazale H, Ripoll C, Leventoux N, Jacob L, Azar S, Mamaeva D, Glasson Y, Calvo C-F, Thomas J-L, Meneceur S, Lallemand Y, Rigau V, Perrin FE, Noristani HN, Rocamonde B, Huillard E, Bauchet L, Hugnot J-P (2019) RNA Profiling of the Human and Mouse Spinal Cord Stem Cell Niches Reveals an Embryonic-like Regionalization with MSX1+ Roof-Plate-Derived Cells. Stem Cell Reports 12:1159–1177.

Hamilton LK, Truong MKV, Bednarczyk MR, Aumont A, Fernandes KJL (2009) Cellular organization of the central canal ependymal zone, a niche of latent neural stem cells in the adult mammalian spinal cord. Neuroscience 164:1044–1056.

Hubbard JM, Böhm UL, Prendergast A, Tseng P-EB, Newman M, Stokes C, Wyart C (2016) Intraspinal Sensory Neurons Provide Powerful Inhibition to Motor Circuits Ensuring Postural Control during Locomotion. Curr Biol 26:2841–2853.

Jalalvand E, Robertson B, Tostivint H, Wallén P, Grillner S (2016a) The Spinal Cord Has an Intrinsic System for the Control of pH. Curr Biol 26:1346–1351.

Jalalvand E, Robertson B, Wallén P, Grillner S (2016b) Ciliated neurons lining the central canal sense both fluid movement and pH through ASIC3. Nat Commun 7:10002.

Jalalvand E, Robertson B, Wallén P, Hill RH, Grillner S (2014) Laterally projecting cerebrospinal fluid-contacting cells in the lamprey spinal cord are of two distinct types. J Comp Neurol 522:1753–1768.

Jurčić N, Er-Raoui G, Airault C, Trouslard J, Wanaverbecq N, Seddik R (2019) GABAB receptors modulate Ca2+ but not G protein-gated inwardly rectifying K+ channels in cerebrospinal-fluid contacting neurones of mouse brainstem. J Physiol (Lond) 597:631–651.

Jurčić N, Michelle C, Trouslard J, Wanaverbecq N, Kastner A (2021) Evidence for PKD2L1-positive neurons distant from the central canal in the ventromedial spinal cord and medulla of the adult mouse. Eur J Neurosci.

Kutna V, Sevc J, Gombalová Z, Matiašová A, Daxnerová Z (2013) Enigmatic cerebrospinal fluid-contacting neurons arise even after the termination of neurogenesis in the rat spinal cord during embryonic development and retain their immature-like characteristics until adulthood. Acta Histochem.

LaMotte CC (1987) Vasoactive intestinal polypeptide cerebrospinal fluid-contacting neurons of the monkey and cat spinal central canal. J Comp Neurol 258:527–541.

Marichal N, García G, Radmilovich M, Trujillo-Cenóz O, Russo RE (2009) Enigmatic central canal contacting cells: immature neurons in “standby mode”? J Neurosci 29:10010–10024.

Marichal N, García G, Radmilovich M, Trujillo-Cenóz O, Russo RE (2012) Spatial domains of progenitor-like cells and functional complexity of a stem cell niche in the neonatal rat spinal cord. Stem Cells 30:2020–2031.

Meletis K, Barnabé-Heider F, Carlén M, Evergren E, Tomilin N, Shupliakov O, Frisén J (2008) Spinal cord injury reveals multilineage differentiation of ependymal cells. PLoS Biol 6:e182.

Nakamura Y, Kurabe M, Matsumoto M, Sato T, Miytashita S, Hoshina K, Kamiya Y, Tainaka K, Matsuzawa H, Ohno N, Ueno M (2023) Cerebrospinal fluid-contacting neuron tracing reveals structural and functional connectivity for locomotion in the mouse spinal cord. Elife 12:e83108.

Orts Del’Immagine A, Seddik R, Tell F, Airault C, Er-Raoui G, Najimi M, Trouslard J, Wanaverbecq N (2015) A single polycystic kidney disease 2-like 1 channel opening acts as a spike generator in cerebrospinal fluid-contacting neurons of adult mouse brainstem. Neuropharmacology.

Orts-Del’Immagine A, Cantaut-Belarif Y, Thouvenin O, Roussel J, Baskaran A, Langui D, Koëth F, Bivas P, Lejeune F-X, Bardet P-L, Wyart C (2020) Sensory Neurons Contacting the Cerebrospinal Fluid Require the Reissner Fiber to Detect Spinal Curvature In Vivo. Curr Biol 30:827-839.e4.

Orts-Del’Immagine A, Kastner A, Tillement V, Tardivel C, Trouslard J, Wanaverbecq N (2014) Morphology, distribution and phenotype of polycystin kidney disease 2-like 1-positive cerebrospinal fluid contacting neurons in the brainstem of adult mice. PLoS ONE 9:e87748.

Orts-Del’Immagine A, Trouslard J, Airault C, Hugnot J-P, Cordier B, Doan T, Kastner A, Wanaverbecq N (2017) Postnatal maturation of mouse medullo-spinal cerebrospinal fluid-contacting neurons. Neuroscience 343:39–54.

Petracca YL, Sartoretti MM, Di Bella DJ, Marin-Burgin A, Carcagno AL, Schinder AF, Lanuza GM (2016) The late and dual origin of cerebrospinal fluid-contacting neurons in the mouse spinal cord. Development 143:880–891.

Pinheiro P, Gering M, Patient R (2004) The basic helix-loop-helix transcription factor, Tal2, marks the lateral floor plate of the spinal cord in zebrafish. Gene Expr Patterns 4:85–92.

Sabelström H, Stenudd M, Réu P, Dias DO, Elfineh M, Zdunek S, Damberg P, Göritz C, Frisén J (2013) Resident neural stem cells restrict tissue damage and neuronal loss after spinal cord injury in mice. Science 342:637–640.

Sabourin J-C, Ackema KB, Ohayon D, Guichet P-O, Perrin FE, Garces A, Ripoll C, Charité J, Simonneau L, Kettenmann H, Zine A, Privat A, Valmier J, Pattyn A, Hugnot J-P (2009) A mesenchymal-like ZEB1(+) niche harbors dorsal radial glial fibrillary acidic protein-positive stem cells in the spinal cord. Stem Cells 27:2722–2733.

Sasaki Y, Ohsawa K, Kanazawa H, Kohsaka S, Imai Y (2001) Iba1 is an actin-cross-linking protein in macrophages/microglia. Biochem Biophys Res Commun 286:292–297.

Sternberg JR, Prendergast AE, Brosse L, Cantaut-Belarif Y, Thouvenin O, Orts-Del'Immagine A, Castillo L, Djenoune L, Kurisu S, McDearmid JR, Bardet P-L, Boccara C, Okamoto H, Delmas P, Wyart C (2018) Pkd2l1 is required for mechanoception in cerebrospinal fluid-contacting neurons and maintenance of spine curvature. Nat Commun 9:3804.

Stoeckel M-E, Uhl-Bronner S, Hugel S, Veinante P, Klein M-J, Mutterer J, Freund-Mercier M-J, Schlichter R (2003) Cerebrospinal fluid-contacting neurons in the rat spinal cord, a gamma-aminobutyric acidergic system expressing the P2X2 subunit of purinergic receptors, PSA-NCAM, and GAP-43 immunoreactivities: light and electron microscopic study. J Comp Neurol 457:159–174.

Tonelli Gombalová Z, Košuth J, Alexovič Matiašová A, Zrubáková J, Žežula I, Giallongo T, Di Giulio AM, Carelli S, Tomašková L, Daxnerová Z, Ševc J (2020) Majority of cerebrospinal fluid-contacting neurons in the spinal cord of C57Bl/6N mice is present in ectopic position unlike in other studied experimental mice strains and mammalian species. J Comp Neurol.

Vígh B, Manzano e Silva MJ, Frank CL, Vincze C, Czirok SJ, Szabó A, Lukáts A, Szél A (2004) The system of cerebrospinal fluid-contacting neurons. Its supposed role in the nonsynaptic signal transmission of the brain. Histol Histopathol 19:607–628.

Yasui K, Hashizume Y, Yoshida M, Kameyama T, Sobue G (1999) Age-related morphologic changes of the central canal of the human spinal cord. Acta Neuropathol 97:253–259.

[MATERIAL & METHODS]

Animals

Experiments were conducted on 5 adult *Macaca mulatta* (Rh. Monkey; weight between 2 and 7 Kg) that have been used in experimental protocols carried out in the institute for other projects. To comply with the 3Rs rules, they were made available at the end of these procedure to collect medullo-spinal tissues. Housing condition and all experiments were conducted in conformity with the rules set by the EC Council Directive (2010/63/UE) and the French "*Direction Départementale de la Protection des Populations des Bouches-du- Rhône* (DDPP13)".

Anesthesia was induced with an injection of zoletil (10 $mg.Kg^{-1}$), xylazine (1 $mg.Kg^{-1}$) and buprenorphine (0.03 $mg.Kg^{-1}$). Following confirmation of full reflexes loss, an intravenous

injection of pentobarbital (100mg.Kg^{-1}) was performed. Upon confirmation of respiratory and cardiac arrest, transcardiac perfusion was carried out. For immunohistology on rodent tissues, 6-week-old mice (3 animals) and 3 month-old rats were injected 30 minutes prior to the procedure with the non-steroidal anti-inflammatory Metacam (5 mg.Kg^{-1}) and subsequently anesthetized with intraperitoneal administration of 100 mg.Kg^{-1}ketamine (Carros, France) and 10 mg.Kg^{-1} xylazine (Puteau, France). Before skin incisions, the local antalgic Lurocaine (5 mg.Kg^{-1}) was injected subcutaneously. Animals transcardially perfused initially with 0.1 M PBS followed by 4% paraformaldehyde (PFA; Sigma-Aldrich) in PBS solution. Tissues were immediately collected, separated in the segments of interest samples (medulla, cervical, thoracic, lumbar, and sacral levels), post-fixed in PBS-4% PFA at 4°C overnight, cryoprotected for several days in 30% sucrose at 4°C and finally frozen in isopentane (−40°C).

Immunohistochemistry

Transverse and longitudinal thin sections (30 µm) were prepared using a cryostat (Leika CM3050) and collected serially in 24-well plates containing 0.1M PBS. For further conservation, sections were transferred in a cryoprotecting solution at -20°C until use. For immunohistochemistry, sections were washed in PBS, incubated first 1h in PBS containing 0.3% Triton X-100 (Sigma) and then in a blocking solution containing 3% horse or goat normal serum and 1% bovine serum albumin (BSA). Sections were incubated overnight at 4°C with primary antibodies (see list in Table 2) in an incubation medium (PBS with 3% horse or goat normal serum). Sections were then washed at least 3 times in PBS and incubated for 2h with secondary antibodies conjugated to either AlexaFluor 488, 594, or 647 (Life Technologies; See Table 2 for details) and finally washed in PBS several times. When more than one primary antibody was used in an immunohistofluorescence labeling experiments, the primary antibodies were applied sequentially. Sections were mounted on polylysine coated slides and coverslipped with a mounting medium for fluorescence microscope preparation (generally after DAPI

staining). To assess the selectively of the observed immunolabelling, in each set of experiments, some sections were treated in the absence of primary antibodies (negative control). Each experiment was performed on tissues obtained from 2-3 animals and analyzed on 3-6 sections for each segment of interest and for each animal (for one SC region). Most antibodies (NeuN, GFAP, Vim, β3-Tub, DCX, Nkx6.1, MAP2, PKD2L1) have been previously used in our studies in mice (Orts-Del'Immagine et al., 2014; Jurčić et al., 2021) and were validated in Rh. monkey by the labelling observed in similar cell populations as in rodent as well as positive labelling for NeuN, MAP2, ChAT, β3-Tubuline, NFH, NF-160 and synaptophysin in neurons and neuronal elements present in the same section away from the cc. Vimentin, GFAP, Iba1 immunofluorescence was detected as expected in ependymal cells, astrocytes or microglial cells, respectively. The antibodies Sox2, Pax6, p27Kip1 were validated by the expected immunolabelling of the cc ependymal stem cell population. Selectivity of the immunostaining was confirmed by the absence of fluorescence when using secondary antibodies alone.

Image acquisition and analysis

Sections were observed on a confocal laser scanning microscope (CLSM; Zeiss LSM700) equipped with solid state fiber optic lasers and single plane images or stacks of images were acquired with a 0.5-1x digital zoom using a 20x objective (numerical aperture, NA: 0.8 for an optical thickness of ~2 µm). Images were acquired at optimal resolution of 1024×1024 pixels. When using 2-4 fluorochromes with different excitation/emission spectra, images were acquired sequentially for each channel (488 nm, green; 555 nm, red; 405 nm, blue; 639 nm, magenta) and the filters and photomultiplier tubes settings chosen to optimize images and avoid signal crosstalk. Images were analyzed and prepared using ZEN 2009 light Edition (Zeiss software), ImageJ 1.45 (NIH) and Corel Photo-Paint. For better visualization, contrast and brightness were adjusted in images used for the figures. Orthogonal projection and co-expression analysis were

performed in Image J using dedicated plugins. Images illustrated at low magnification were obtained using the ZEN 2009 mosaic routine (from 4 x 4 to 6 x 6 fields of view) while high magnification images were obtained from z-projection of 5 to 12 images in a stack. For quantification analysis of the cell density, MAP2+ CSF-cNs were counted manually in each image and the total cell number divided by the section thickness (10 µm stack depth). For the analysis of peri-ependymal zone width, cc area (10^3 x μm^2), CSF-cN distance to the cc, the measures were performed using ImageJ. At each medullo-spinal level, the analysis was performed in 3-4 animals on at least 6 different sections per animal.

Statistical analysis

All data presented in Fig. 5 are expressed as mean ± SD and represented as whisker boxplots using the Tukey's method as well as with “violin” plots to illustrate data point density and the data point distribution. In whisker plots, for each data set, the median and the 25th to the 75th percentiles (lower and upper limits of each bar, respectively) are calculated. Next, the interquartile distance (IQR) is determined as the difference between the 25th and 75th percentiles, and the whiskers limits, or “inner fences” calculated as the 75th percentile plus 1.5 times IQR and the 25th percentile minus 1.5 times IQR. We compared one parameter (PEZ width, CC area, CSF-cN number or distance to the cc) across several medullo-spinal segments, here labeled as *Region*. In one animal, the parameters measured in each *Region* are assumed dependent from the organization of the other regions, and the variable *Region* represents a dependent factor. On the other hand, the same variables represent independent factors when considered in different animals. Therefore, the statistical analyses required using a nonlinear mixed effect (nlme) model taking into account in a hierarchical way both dependent and independent variables as well as the interaction between the variables. Finally, the choice of animals used for this study was done randomly among all those available; therefore, it is

necessary to implement the statistical model with a factor corresponding to this random effect. The statistical analyses were carried out using the R Studio 3.3.1 statistical software (R Studio Team, 2015) in the R environment and the “non-linear mixed effect (nlme version 3.1–128)” package (Pinheiro et al., 2004). The null hypothesis was set as the absence of difference between the data among each group. The nlme model was tested using an analysis of the variance (ANOVA), and a subsequent post-hoc Sidak test for multiple pairwise comparison. We provide the values for $\chi 2$, the degree of freedom (number of parameters −1, dF) and the p-values for the given fixed factor tested. Statistical differences were considered as significant for $p < 0.05$.

[ADDITIONAL INFORMATION]

Data availability statement

The data of this manuscript are available upon request.

Competing interests

The authors declare no competing financial interests.

Authors contributions

All experiments were performed at the ‘Institut des Neurosciences de la Timone (INT)’ of Aix-Marseille University. Conception and design of the work: AK & NW. Acquisition, analysis, and interpretation of data for the work: AK & NW. Drafting the work or revising it critically for important intellectual content: AK & NW. All authors have read and approved the final version of this manuscript and agree to be accountable for all aspects of the work in ensuring that questions related to the accuracy or integrity of any part of the work are appropriately investigated and resolved. All persons designated as authors qualify for authorship, and all those who qualify for authorship are listed.

Funding

This research was supported by funding obtained from Aix-Marseille University (AMU), le Centre National pour la Recherche Scientifique (CNRS – INSB) and l'Agence National pour la Recherche (ANR-PRC-ANR-20-CE14-0042, MotoNeuroMod; NW).

Acknowledgments

We gratefully thank Caroline Blanc-Tailleur and Jorge Jose Franco-Ramirez for their assistance in immunohistochemistry experiments and analysis as well as SpiCCI team members for carefull proof reading and comments. We acknowledge the 'Institut de Neurosciences de la Timone (INT)' technical facilities for their support in the study (NeuroBioTools/ConnectoVir: Molecular Biology and Histology; INPHIM: confocal microscopy) and the Mediterranean Primate Research Centre (MPRC).

[FIGURE LEGENDS]

Figure 1: The region around the central canal is enriched with astrocytes and ependymal cell radiating fibers with only few neuronal elements.

(**A1-D1**) Low magnification micrographs illustrating around the central canal the expression of vimentin (Vim), a marker for ependymal cells (EC) and fibers, along with neuronal markers (NFH, **A1** and NF-160, **B1**), neuronal nucleus protein (NeuN, **C1**) and astrocytic markers (GFAP, **D1)** in transverse thin sections obtained from the caudal cervical segment of the Rh. monkey spinal cord.

(**A2-4**) High magnification images from **A1** for the region around the central canal (cc) indicating the presence of long radiating Vim positive fibers originating from soma in the ependymal cells layer (ECL) and extending to form the peri-ependymal zone (PEZ, **A2**). (**A3**) Immunolabelling

against NFH to reveal neuronal elements around the cc. (**A4**) Merged image showing the distribution of vimentin and NFH along with DAPI, a nuclear marker. Note the presence around the cc of the PEZ delineated by Vim+ radiating fibers and largely devoid of neuronal elements.

(**B2-4**) High magnification images from **B1** showing Vim (**B2**) and NF-160 (**B3**) labelling, respectively, to visualize EC and axons. The merged image in **B4** illustrates the organization of axonal fibers in the grey matter and around the PEZ. Note the absence of NF-160 positive fibers within the PEZ as well as the presence of numerous *puncta* in the dorsal region of the white matter corresponding to longitudinal axonal projection.

(**C2-4**) High magnification images from **C1** illustrating Vim (**C2**) and NeuN (**C3,** arrows in **C3** and **C4**), distribution around the cc. The merged image in **C4** confirms the absence of mature neurons within the PEZ.

(**D2-4**) High magnification images from **D1** showing the distribution of Vim (**D2**) and GFAP, a astrocytic marker (**D3**). The merged image in **D4** indicates the presence of a region around the cc that is delineated by vimentin positive fibers and enriched with astrocytes.

Sections are oriented with the dorsal region on top and the regions illustrated in high magnification images corresponds to those indicated with yellow boxes in the low magnification images on the left. Color code for the labels on top of images corresponds to the illustrated markers. Dashed lines in A1 to D1 delineates the grey matter (GM) from the white matter (WM) with the dorsal and ventral horns. Scale bars are shown in the images left and right. Dashed lines: cc; Full lines: ECL; Doted-dashed lines: PEZ.

Figure 2: The PEZ contains CSF-contacting neurons, the only neurons present in this region.

(**A1**) Low magnification micrographs illustrating the distribution of vimentin (Vim), to reveal EC and fibers, and MAP2, a marker for the somato-dendritic compartments, in one transverse thin section obtained from the caudal cervical segment of the spinal cord. Note that MAP2 is intensively expressed in the whole GM. (**A2**) MAP2 immunolabelling reveals the presence of neurons in the PEZ. These neurons exhibit the characteristic morphology of CSF-contacting neurons (CSF-cNs), with a small soma (arrows) localized around the cc and projecting a single large dendrite (arrowheads) ended with a round protrusion or bud (asterisks) in the cc lumen. Note also the intense MAP2 immunolabelling outside the PEZ, in the GM. The merged image in **A3** shows that CSF-cNs (MAP2) are the only neurons present in the PEZ and extend their dendrites along the Vim positive fibers. DAPI: nuclear marker.

(B) MAP2/NFH co-immunolabelling (**B1**) confirming that CSF-cNs are restricted to the NFH negative hyponeuronal PEZ. **(B2)** β3-tubuline (β3-Tub), a marker for somato-dendritic and axonal compartments, along with NFH immunolabelling allows CSF-cN visualization in the PEZ devoid of NFH IR.

(C) Co-immunolabelling against MAP2 and Iba1, a marker for microglial cells, illustrating their presence in the parenchyma, the PEZ (arrowheads) close to CSF-cNs (arrows) as well as around the cc with projection (filled arrows) within the ECL.

(**D**) Horizontal thin section obtained at the level of the cc (dashed lines) of a cervical spinal cord section and immunolabelled against MAP2 (**D1 and 2**) and Vim (**D2**) to reveal CSF-cNs and ependymal cells or fibers, respectively. Note that MAP2 immunolabelling indicates the distribution in the antero-posterior axis of CSF-cNs within the PEZ along vimentin positive fibers.

(**E**) Micrographs illustrating PKD2L1 selective expression in the soma (arrows), dendrite (arrowheads), and bud (asterisk) of CSF-cNs in transverse thin sections prepared from cervical spinal cord.

(**F**) Transverse thin section (caudal cervical level) immunolabelled against β3-Tub (Left) and GAD67 (Right), a selective marker of GABAergic neurons.

For abbreviations see Fig. 1. The region illustrated in the high magnification images in A2 and A3 corresponds to that indicated with a yellow box in A1 (left). Color code for the labels on top of images corresponds to the illustrated markers. Scale bars are shown on the images.

Figure 3: In rodents the ependymal cell layer is contiguous to the parenchyma.

Organization of the region around the cc in sections obtained from mouse (**A, C** and **D**) and rat (**B, D** and **F**) spinal cord.

(**A** and **B**) Images of the astrocyte distribution (GFAP; **A1** and **B1**) along with nuclear labeling (DAPI). (**A2** and **B2**) Merged micrographs showing the distribution for the immunolabelling against GFAP and NFH. Note that in rodent the neural parenchyma is contiguous to the ECL (compare with Fig.s 1 and 2).

(**C** and **D**) Images of the immunolabelling against Vim (**C1** and **D1**) and PKD2L1 (**C2** and **D2**). Note that CSF-cNs selectively express PKD2L1 and are present within or close to the ECL in direct contact with the parenchyma.

(**E** and **F**) Images of the immunolabelling against MAP2 and Vim around the cc (**E1** and **F1**) and against NeuN (**E2** and **F2**). The images confirm the absence of a PEZ in rodent illustrated by the close apposition of MAP2 and Vim labelling and the presence of NeuN immunolabelling close to the cc.

For abbreviations see Fig. 1. Color code for the labels on top of images corresponds to the illustrated markers. Scale bars are shown on the images. Arrows: CSF-cNs.

Figure 4: The PEZ organization observed in Rhesus monkey is conserved along the whole rostro-caudal axis of the central canal.

(A1-**E1**) Micrographs at low magnification illustrating the anatomy of the medulla and the spinal cord (cervical to sacral) along the antero-posterior axis in transverse sections with the characteristic organization of the grey matter at each level. (**A2**-**E2**) High magnification images of the region around the cc from the sections illustrated from A1 to E1 (yellow squares) and showing the immunolabelling against NFH, GFAP and DAPI**.** (**A3**-**E3**) Representative images for the PEZ organization with the presence of CSF-cNs around the cc and labelled with MAP2 and DAPI. (**A4**-**E4**) Images showing the co-immunolabelling against β3-Tub and MAP2 to reveal axonal (β3-Tub only; arrowhead) as well as somato-dendritic compartments (β3-Tub and MAP2).

For abbreviations see Fig. 1. Arrows point to CSF-cNs. Color code for the labels on top of images corresponds to the illustrated markers. Scale bars are shown on the images.

Figure 5: Properties of the peri-ependymal zone (PEZ) and CSF-cNs distribution along the medullo-spinal axis.

Summary graphs for the quantification of the PEZ width (**A**), the cc lumen area ($\mu m^2 \times 10^3$, **B**), the number of CSF-cNs (**C**) and their distance to the cc (**D**) at the medulla (Med), the rostral, mid, and caudal cervical zone (rCerv, mCerv and cCerv), the thoracic (Tho), the lumbar (Lum) and the sacral (Sac) segments. For each graph, whiskers boxplots are presented with superimposed violin plots for the data point density and distribution. Statistical significance was analyzed using a non-linear multi-effect test: (**A**) $\chi^2 = 621.84$, df = 6 and $p(\chi^2) < 2.2 \times 10^{-16}$;(**B**) χ^2

= 56,11, df = 6 and $p(\chi^2) = 2.763 \times 10^{-10}$; (**C**) $\chi^2 = 113.36$, df = 6 and $p(\chi^2) < 2.2 \times 10^{-16}$; (**D**) $\chi^2 = 416.11$, df = 6 and $p(\chi^2) < 2.2 \times 10^{-16}$. Pairwise post-hoc comparison using Sidak method: *, < 0.05; **, < 0.01; ***, < 0.001 and ****<0.0001 (see detail in Table 1).

Figure 6: In Rh. monkey, CSF-cNs exhibit features of immature neurons

(**A**) Representative micrographs illustrating immunolabelling against NeuN alone (**A1**) and with MAP2 (**A2**) around the cc. Asterisk: NeuN positive neurons in the parenchyma; Arrows: CSF-cNs; Inset in A2: enlargement for the zone around the cc highlighted with a yellow box to illustrate at higher magnification that CSF-cNs are NeuN negative (compare A1 and A2).

(**B**) Images illustrating immunolabelling against doublecortine (DCX) alone (**B1**) and with MAP2 (**B2**). Arrows: CSF-cNs; Arrowheads: CSF-cN dendrites; Inset in B1 and 2: enlargement for the zone around the cc highlighted with a yellow box to illustrate at higher magnification DCX/MAP2 co-expression at the somatic and dendritic levels in CSF-cNs (compare B1 and B2).

(**C**) Representative micrographs illustrating immunolabelling against MAP2 alone (**C1**) and with Nkx6.1 (**C2**). Arrows: CSF-cNs. Note that Nkx6.1 is expressed by all CSF-cNs and by EC but is absent in the parenchyma.

(**D**) Immunolabelling against PKD2L1 alone (magenta, Top row) and with Nkx6.1 (green, Bottom row) in transverse section prepared from cervical spinal cord. The data confirms that all CSF-cNs are PKD2L1+ and selectively express Nkx6.1.

(**E**-**F**) Micrographs illustrating the immunolabelling against MAP2 alone (**E1**) or Sox2 alone (**F1**) as well as co-immunolabelling against Sox2 and MAP2 (**E2**) or Sox2 and Vim (**F2**). Note the high Sox2 IR of EC around the cc (**E2** and **F1**) as well as Sox2 selective expression in CSF-cNs (Arrows in **E**).

(**G**-**H**) Micrographs illustrating the immunolabelling against p27Kip1 alone (**G1**) or Pax6 alone (**H1**) as well as co-immunolabelling against p27Kip1 and MAP2 (**G2**) or Pax6 and Vim (**H2**). All CSF-cNs and EC express p27Kip1 while Pax6 is only present in EC. Note the presence in the PEZ of Pax6 positive cell bodies.

Illustrated sections were prepared from spinal cord cervical segments. For abbreviations see Fig. 1 and color code for the labels on top of images corresponds to the illustrated markers. Scale bars are shown on the images.

Figure 7: CSF-cN axons appear immature and to project within the PEZ in the longitudinal axis.

(**A**) Representative images illustrating the immunolabelling against MAP2 alone (**A1)** and with β3-Tub (**A2)** in a transverse or longitudinal (**A3** and **A4**) section. MAP2 labels CSF-cN somato-dendritic compartments while β3-Tub also reveals their axonal projection. In **A2**, note in the PEZ the presence of β3-Tub positive but MAP2 negative patches (arrowheads) and in **A4**, of β3-Tub positive longitudinal fiber bundles (arrowheads) that might correspond to CSF-cN axonal projections.

(**B-C**) Representative images illustrating the immunolabelling against β3-Tub alone (**B1, B3, C1** and **C3**) and co-immunolabelling against β3-Tub and NF-160 (**B2** and **B4**) or NFH (**C2** and **C4**) in transverse (**B1, 2** and **C1, 2**) or longitudinal sections (**B3, 4** and **C3,4**). Note in the PEZ, the presence of β3-Tub positive patches and longitudinal fiber bundles (arrowheads) that are neither NF-160 nor NFH positive. In **C3** and **4**, the section cut with an angle allows visualizing both the CSF-cN cell bodies at the level of the cc (Left) as well as the β3-Tub positive longitudinal fiber bundles (Right) at a more dorsal level.

For abbreviations see Fig. 1. Small arrows: CSF-cN soma; arrowheads: CSF-cN dendrite; filled arrowheads: axonal projection. Color code for the labels on top of images corresponds to the illustrated markers. Scale bars are shown on the images.

Figure 8: CSF-cN neurons receive somato-dendritic GABAergic and serotoninergic synaptic contacts.

(**A**-**B**) Transverse sections showing CSF-cNs (MAP2, red) around the cc and synaptic contacts (synaptophysin, Syn; red) on their soma or dendrites in cervical (**A1)** and thoracic (**B1**) segments (see **A2, 3** and **B2, 3**).

(**C**) GAD67 and Syn co-immunolabelling (cervical SC) showing the presence of GABAergic synaptic contacts (**C1**) around CSF-cN dendrites (see **C2** and **3**).

(**D**) MAP2, serotonin (5-HT) and Syn co-immunolabelling showing the presence of 5-HT positive synaptic contacts (**D1**) around CSF-cNs cell bodies and dendrites (see **D2, 3**) mainly in the dorsal region of the SC.

In **A-D**, Enlargements for the regions highlighted with yellow boxes in **A1-D1** and the respective orthogonal projections (along the YZ axis: 1 and 1' and the XZ axis: 2 and 2', see labels). White, blue, and yellow arrows indicate CSF-cN soma, syn positive and GAD (**C**) or 5-HT (**D**) positive puncta, respectively. For abbreviations see Fig. 1. Color code for the labels on top of images corresponds to the illustrated markers. DAPI is presented in white. Scale bars are shown on the images.

[TABLES]

Table 1: Quantitative analysis of the Peri-ependymal Zone and CSF-cNs properties

A - Peri-ependymal zone Width (µm)						
Med	**rCerv**	**mCerv**	**cCerv**	**Tho**	**Lum**	**Sac**
88 ± 11	59 ± 15	54 ± 9	79 ± 19	33 ± 9 µm	31 ± 8	38 ± 7
S=18	S=36	S=29	S=42	S=27	S=30	S=35
B - Central canal Area (x 10^3 µm^2)						
Med	**rCerv**	**mCerv**	**cCerv**	**Tho**	**Lum**	**Sac**
6.6 ± 3.0	4.0 ± 1.8	2.8 ± 2.4	4.7 ± 2.8	2.7 ± 3.3	4.7 ± 3.9	6.0 ± 2.0
S=37	S=41	S=44	S=44	S=55	S=26	S=13
C- CSF-cN Density (cell number/10 µm tissue depth)						
Med	**rCerv**	**mCerv**	**cCerv**	**Tho**	**Lum**	**Sac**
7 ± 4	8 ± 3	12 ± 3	14 ± 4	9 ± 4	8 ± 4	10 ± 3
S=32	S=57	S=32	S=51	S=42	S=29	S=18
D - CSF-cN Distance to Central canal (µm)						
Med	**rCerv**	**mCerv**	**cCerv**	**Tho**	**Lum**	**Sac**
56 ± 28	47 ± 25	52 ± 29	33 ± 22	22 ± 19	18 ± 16	26 ± 16
n=130	n= 373	n=321	n=469	n=209	n=154	n=171
S=32	S=57	S=32	S=51	S=42	S=29	S=18
S=10 to 22				S=10 to 24		

Med: medulla; r, m and c Cerv: rostral, mid and caudal Cervical; Tho: Thoracic, Lum: Lumbar and Sac: Sacral
Animals: 2 for Med or Sac; 3 or 4 for all other segments; S: Number of sections; n: number of cells. Data as mean ± SD; *Non-linear multi effect* (nlme) statistical test.

Table 2: List of primary antibodies used for immunolabelling

Antibodies	Distributor	Reference	Host	Dilution
β3-tubuline/ TUJ1	Sigma	T2200	rabbit	1:500
β3-tubuline TUJ1	Biolegend	801213	mouse	1:500
ChAT	Millipore	AB144P	goat	1:100
DCX	Santa Cruz	SC-8066	goat	1:100
GAD67	Millipore	MAB5406	mouse	1:500
GFAP	Sigma	G3893	mouse	1:500
GFAP	Dako	Z0334	rabbit	1:500
5-HT	Immunostar	20079	goat	1:500
Iba1	Wako	019-19741	rabbit	1:800
MAP2	Sigma	M-1406	mouse	1:600
NeuN	Millipore	MAB377	mouse	1:800
NF-160	Sigma	N5264	mouse	1:1000
NFH SMI32	Biolegend	801702	mouse	1:500
Nkx6.1	DSHB	F55A10	mouse	1:100
P27Kip1	Epitomics	2187	rabbit	1:200
Pax6	Santa Cruz	Sc-53108	mouse	1:100
PKD2L1	Millipore	AB9084	rabbit	1:700
Sox2	Santa Cruz	Sc-365823	mouse	1:200
Synaptophysin	Epitomics	1485	rabbit	1:500
V-Glut	Millipore	ABN1647	rabbit	1:200
Vimentine	Millipore	AB5733	Chicken	1:700

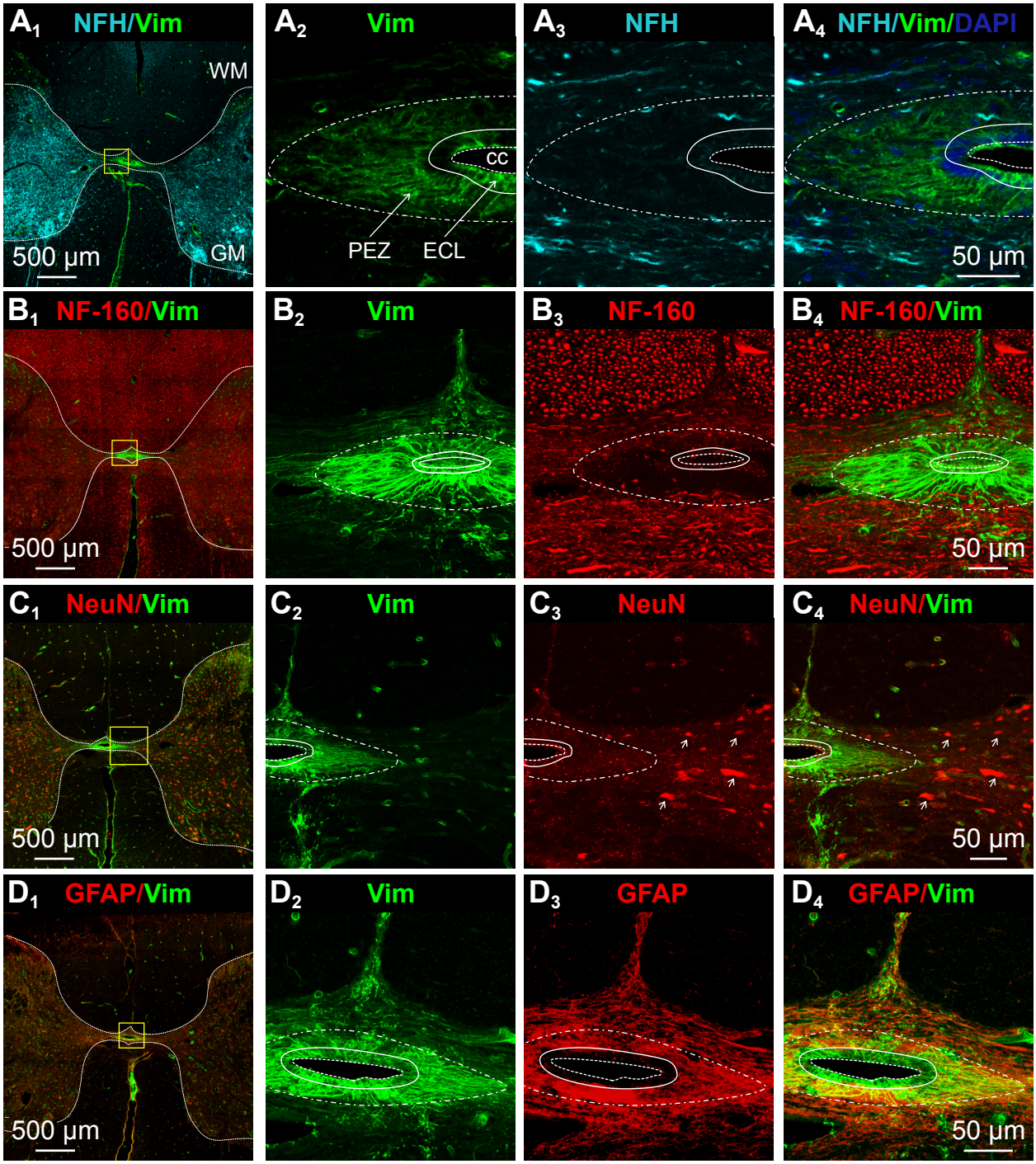
A1 NFH/Vim
WM
GM
500 μm
A2 Vim
CC
PEZ
ECL
A3 NFH
A4 NFH/Vim/DAPI
50 μm
B1 NF-160/Vim
500 μm
B2 Vim
B3 NF-160
B4 NF-160/Vim
50 μm
C1 NeuN/Vim
500 μm
C2 Vim
C3 NeuN
C4 NeuN/Vim
50 μm
D1 GFAP/Vim
500 μm
D2 Vim
D3 GFAP
D4 GFAP/Vim
50 μm

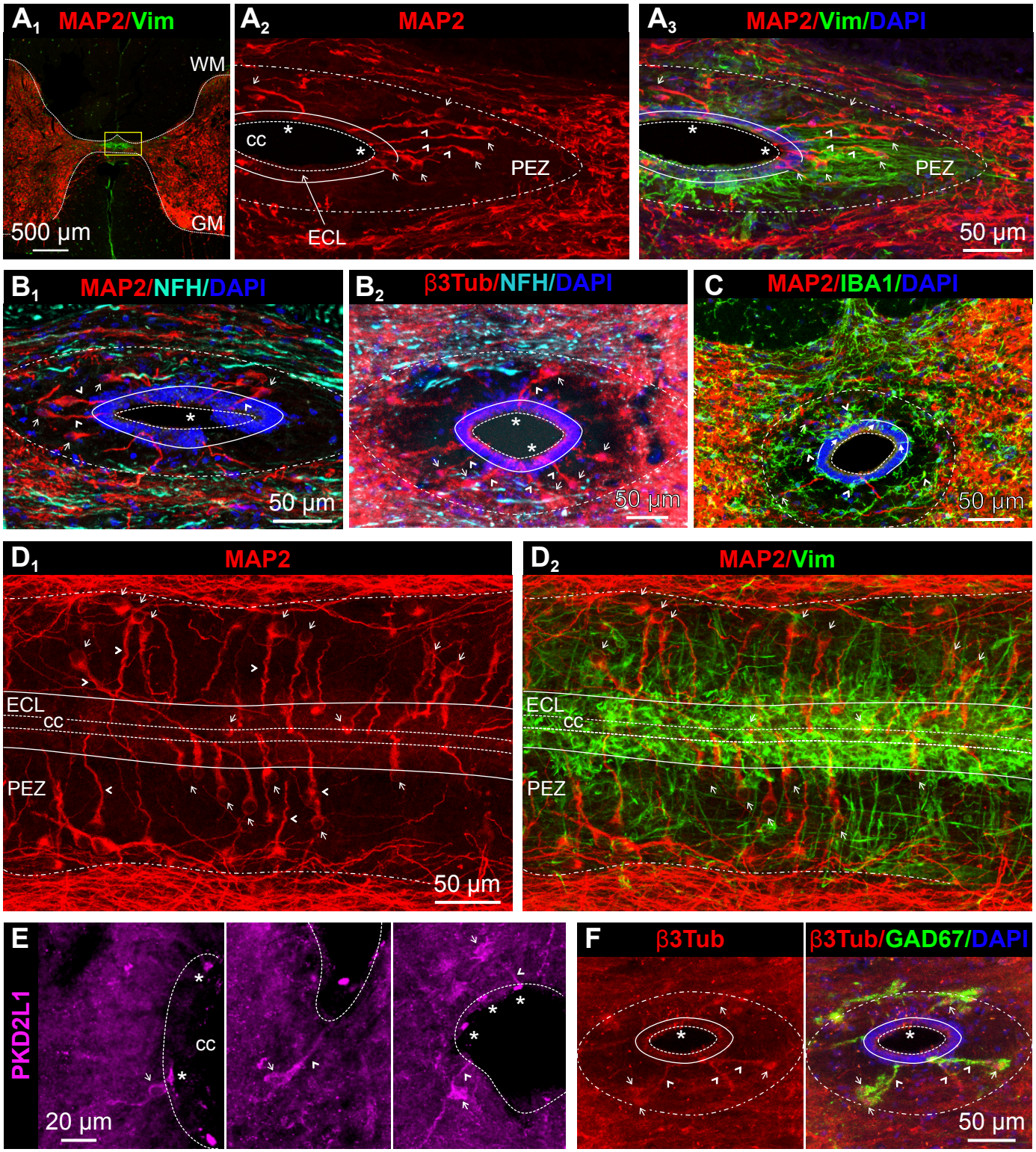
A1 MAP2/Vim
WM
GM
500 µm
A2 MAP2
cc
PEZ
ECL
A3 MAP2/Vim/DAPI
PEZ
50 µm
B1 MAP2/NFH/DAPI
50 µm
B2 β3Tub/NFH/DAPI
50 µm
C MAP2/IBA1/DAPI
50 µm
D1 MAP2
ECL
cc
PEZ
50 µm
D2 MAP2/Vim
ECL
cc
PEZ
E
PKD2L1
cc
20 µm
F β3Tub
β3Tub/GAD67/DAPI
50 µm

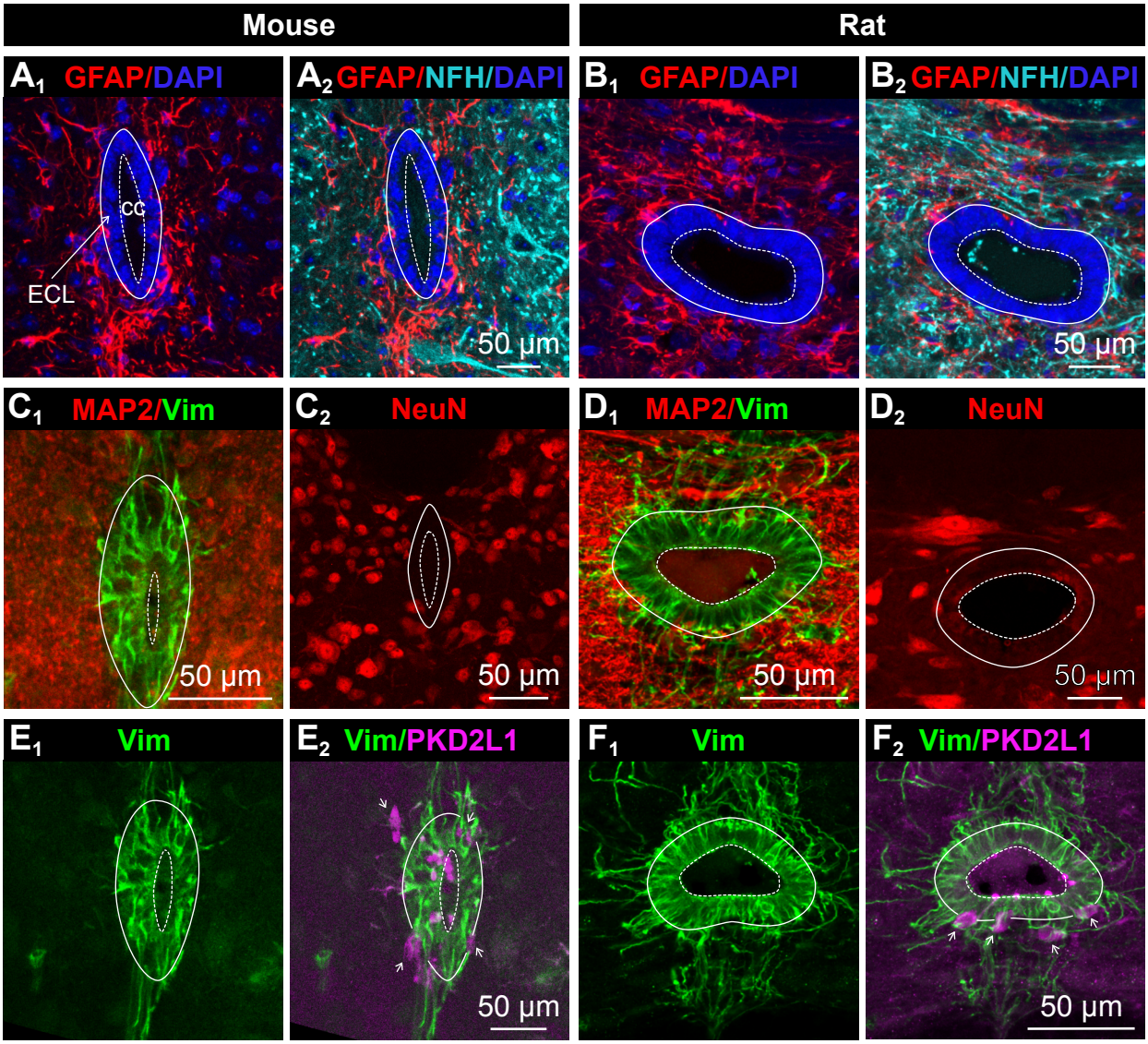
Mouse
Rat
A1 GFAP/DAPI
CC
ECL
A2 GFAP/NFH/DAPI
50 μm
B1 GFAP/DAPI
B2 GFAP/NFH/DAPI
50 μm
C1 MAP2/Vim
50 μm
C2 NeuN
50 μm
D1 MAP2/Vim
50 μm
D2 NeuN
50 μm
E1 Vim
E2 Vim/PKD2L1
50 μm
F1 Vim
F2 Vim/PKD2L1
50 μm

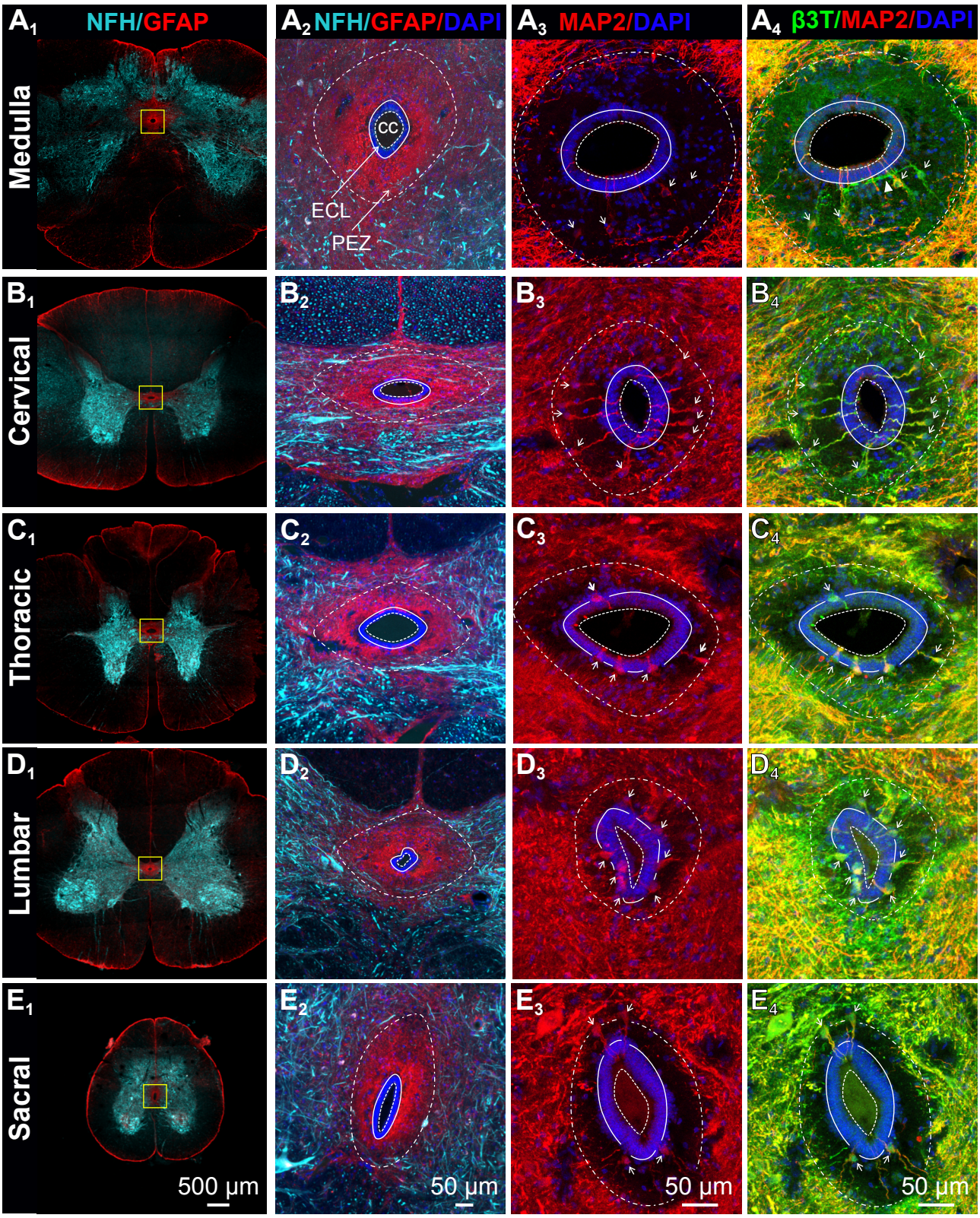
A1 NFH/GFAP
A2 NFH/GFAP/DAPI
A3 MAP2/DAPI
A4 β3T/MAP2/DAPI
Medulla
CC
ECL
PEZ
B1
B2
B3
B4
Cervical
C1
C2
C3
C4
Thoracic
D1
D2
D3
D4
Lumbar
E1
E2
E3
E4
Sacral
500 μm
50 μm
50 μm
50 μm

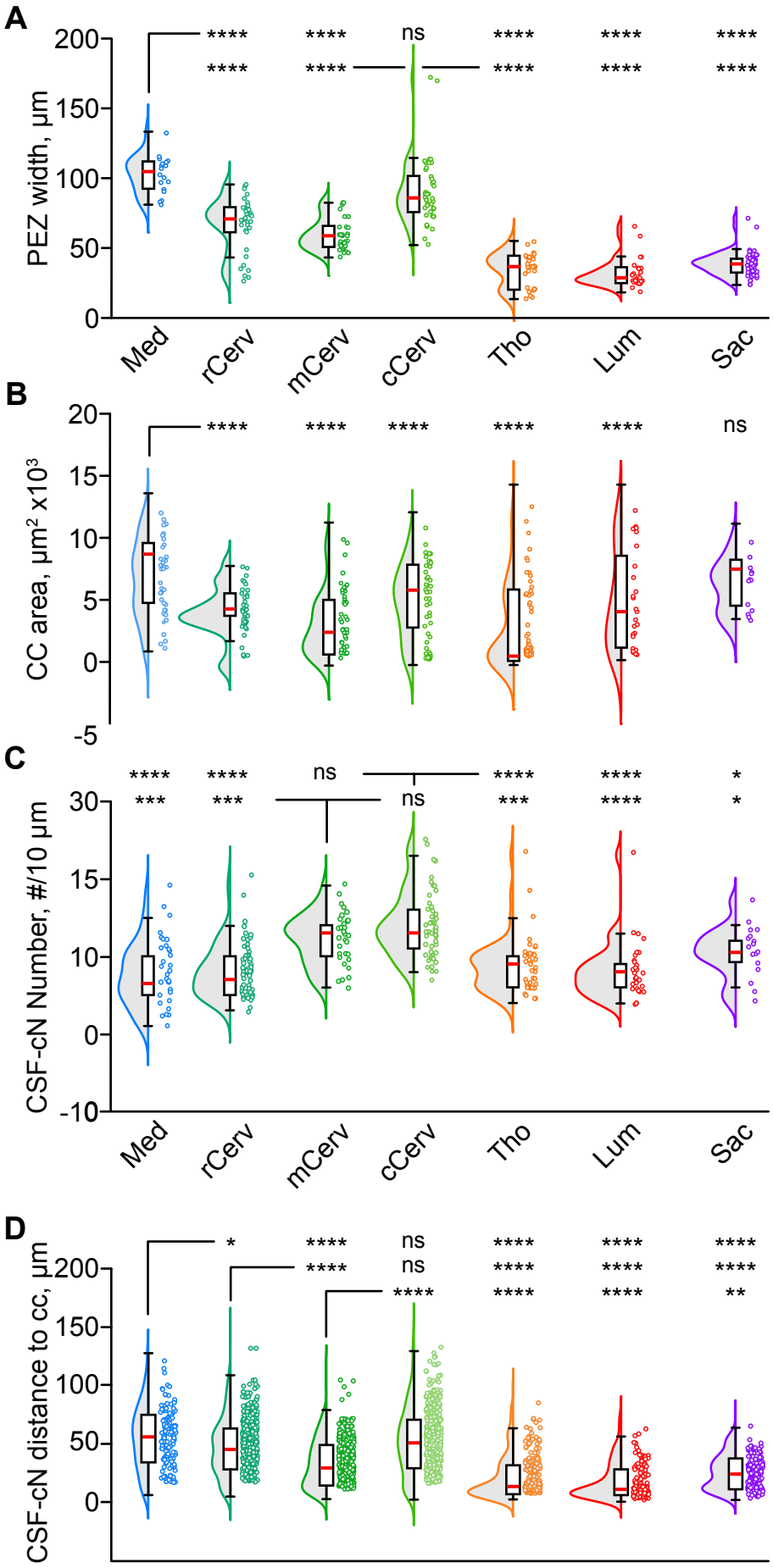
A
PEZ width, µm
200
150
100
50
0
****
****
****
****
ns
****
****
****
****
****
****
****
Med
rCerv
mCerv
cCerv
Tho
Lum
Sac
B
CC area, µm² x10³
20
15
10
5
0
-5
****
****
****
****
****
ns
C
CSF-cN Number, #/10 µm
30
15
10
0
-10
****
***
****
***
ns
ns
****
***
****
****
*
*
Med
rCerv
mCerv
cCerv
Tho
Lum
Sac
D
CSF-cN distance to cc, µm
200
150
100
50
0
*
****
****
ns
ns
****
****
****
****
****
****
****
****
****
**

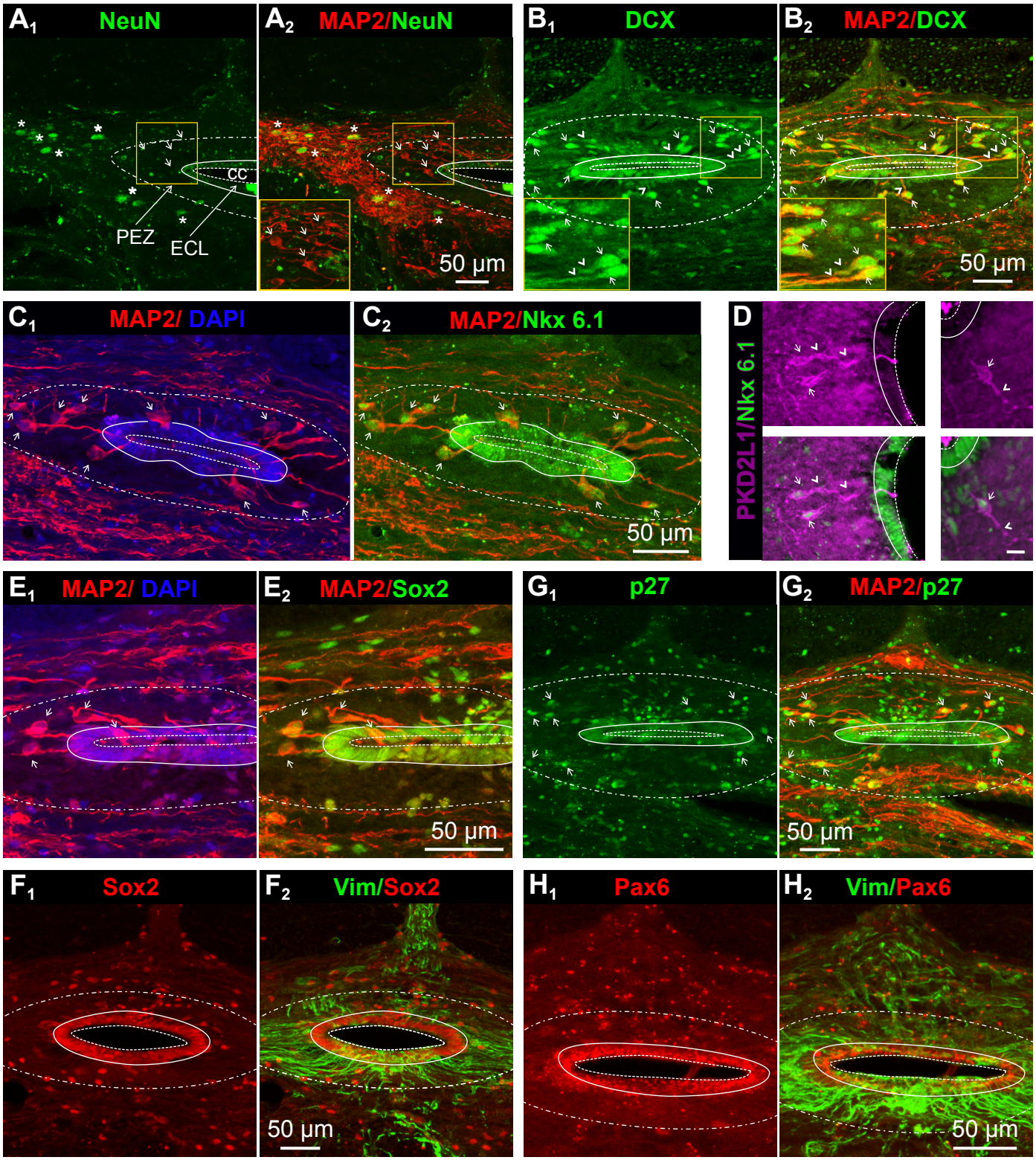
A1
NeuN
CC
PEZ
ECL
A2
MAP2/NeuN
50 µm
B1
DCX
B2
MAP2/DCX
50 µm
C1
MAP2/ DAPI
C2
MAP2/Nkx 6.1
50 µm
D
PKD2L1/Nkx 6.1
E1
MAP2/ DAPI
E2
MAP2/Sox2
50 µm
G1
p27
G2
MAP2/p27
50 µm
F1
Sox2
F2
Vim/Sox2
50 µm
H1
Pax6
H2
Vim/Pax6
50 µm

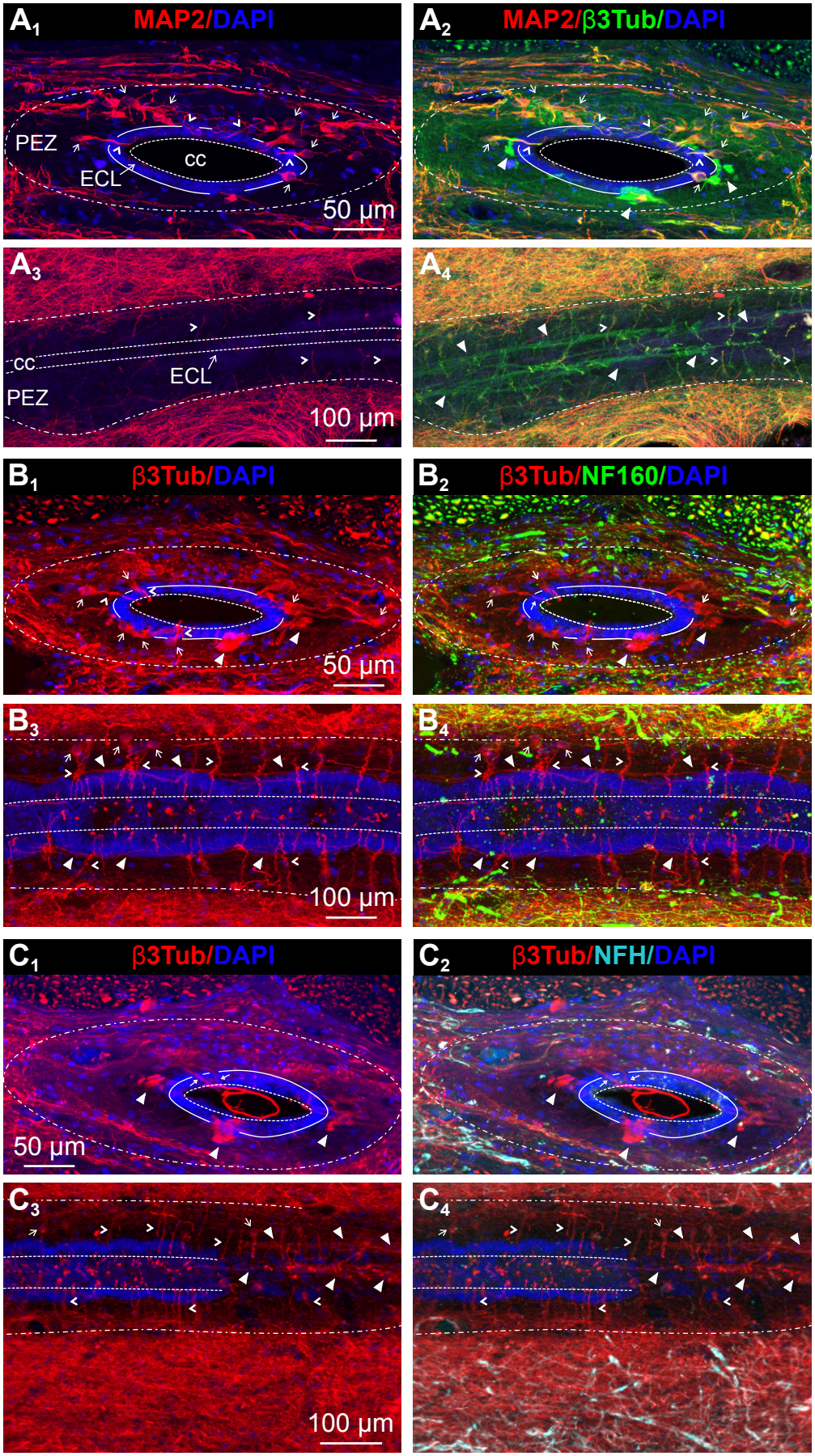
A1
MAP2/DAPI
PEZ
ECL
cc
50 µm
A2
MAP2/β3Tub/DAPI
A3
cc
ECL
PEZ
100 µm
A4
B1
β3Tub/DAPI
50 µm
B2
β3Tub/NF160/DAPI
B3
100 µm
B4
C1
β3Tub/DAPI
50 µm
C2
β3Tub/NFH/DAPI
C3
100 µm
C4

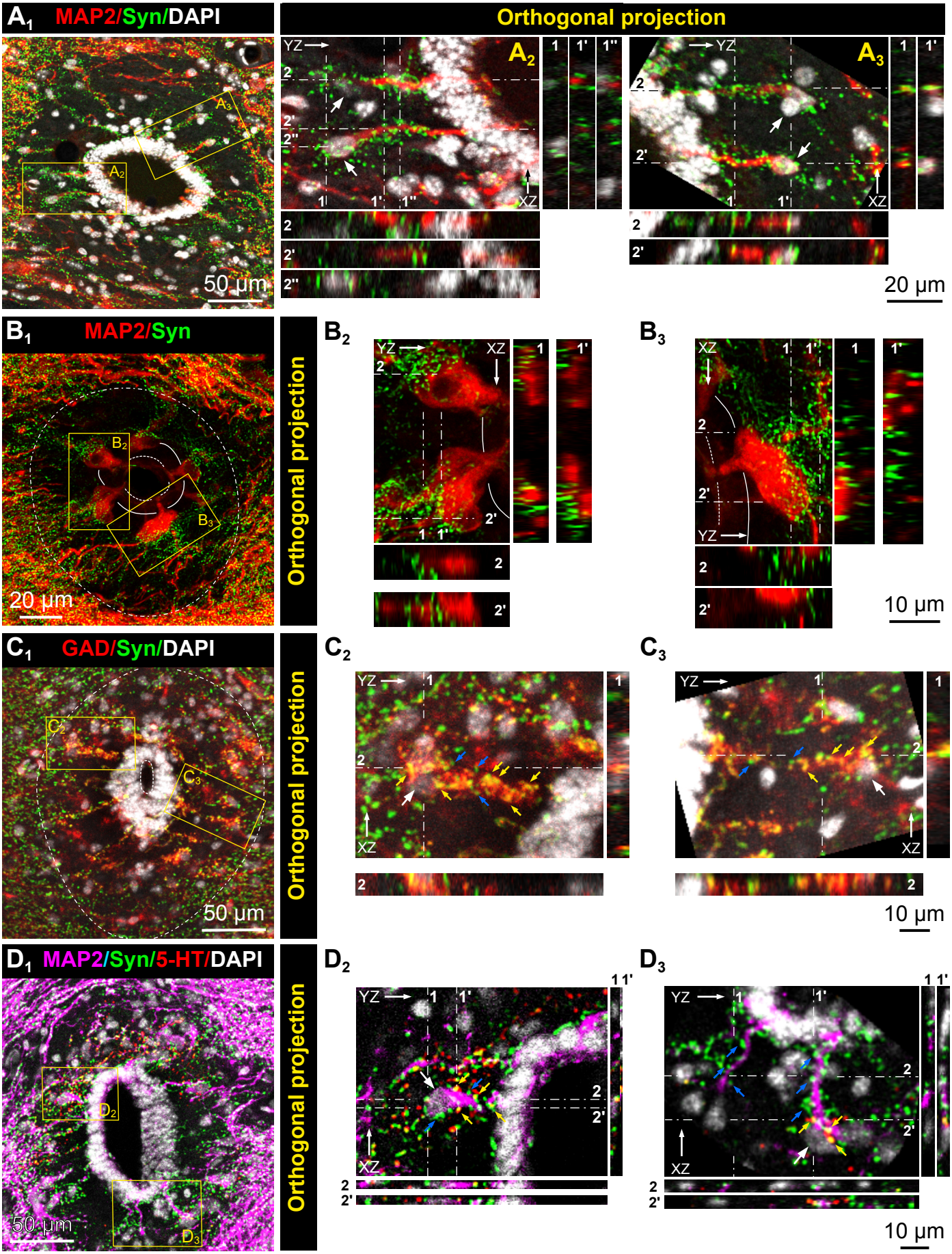
A1 MAP2/Syn/DAPI
Orthogonal projection
A2
A3
50 µm
20 µm
B1 MAP2/Syn
Orthogonal projection
B2
B3
20 µm
10 µm
C1 GAD/Syn/DAPI
Orthogonal projection
C2
C3
50 µm
10 µm
D1 MAP2/Syn/5-HT/DAPI
Orthogonal projection
D2
D3
50 µm
10 µm
YZ
XZ